Probing semiconductor band structures and heterojunction interface properties with ballistic carrier emission: GaAs/$Al_xGa_{1-x}As$ as a model system

Wei Yi* and Venkatesh Narayanamurti
School of Engineering and Applied Sciences, Harvard University, Cambridge, Massachusetts 02138, USA

Hong Lu, Michael A. Scarpulla,† and Arthur C. Gossard
Materials Department, University of California, Santa Barbara, California 93106, USA

(Received 6 May 2010; revised manuscript received 7 June 2010; published 24 June 2010)

Utilizing three-terminal tunnel emission of ballistic electrons and holes in a planar tunnel transistor with a Mott-barrier collector, we have developed a method to self-consistently determine the energy gap of a semiconductor and band discontinuities at a semiconductor heterojunction without using *a priori* material parameters. Measurements are performed on lattice-matched GaAs/$Al_xGa_{1-x}As$ (100) single-barrier double heterostructures with $Al_xGa_{1-x}As$ as the model ternary III–V compounds. Electronic band gaps of the AlGaAs alloys and band offsets at the GaAs/AlGaAs (100) interfaces are measured with a resolution of several meV at 4.2 K. The direct-gap Γ band offset ratio for the GaAs/AlGaAs (100) interface is found to be 59:41 (±3%). Reexamination of our previous experiment [W. Yi *et al.*, Appl. Phys. Lett. **95**, 112102 (2009)] revealed that, in the indirect-gap regime, ballistic electrons from direct tunnel emissions probe the X valley in the conduction band, while those from Auger-like scattering processes in the metal base film probe the higher-lying L valley. Such selective electron collection may be explained by their different momentum distributions and parallel momentum conservation at the quasiepitaxial Al/GaAs (100) interface. We argue that the present method is in principle applicable to arbitrary type-I semiconductor heterostructures.

DOI: 10.1103/PhysRevB.81.235325 PACS number(s): 73.40.Kp, 73.21.−b, 73.23.Ad

I. INTRODUCTION

Among the most important properties of semiconductor materials are their energy gaps and the relative alignment of the energy band edges at the heterojunction (HJ) interface between two dissimilar semiconductors, i.e., the way in which the total band gap difference distributes between the conduction band discontinuity ΔE_C and the valence band discontinuity ΔE_V. An accurate knowledge of such properties is crucial for the design of heterostructure devices, which have found wide applications in high speed and power electronics, photonics, and energy conversion. Heterostructures have also led to fundamental breakthroughs, such as integer and fractional Quantum Hall effects, in studies of two-dimensional electron or hole system which may be formed at the heterointerfaces.

Historically numerous efforts have been devoted to measure the band gap and band offsets. In general, band gaps are measured mostly with optical spectroscopies such as absorption, photoluminescence (PL), photoluminescence excitation (PLE), and ellipsometry.[1] Electronic band gap measurements on atomically flat single crystal surfaces were performed with two-terminal tunneling spectroscopy using a scanning tunneling microscope (STM).[2] Band offset measurements can be divided into three categories: electrical techniques such as thermionic emission and capacitance-voltage profiling (C–V); optical techniques such as absorption, PL, and PLE; and photoelectron techniques such as x-ray photoelectron spectroscopy (XPS) and ultraviolet photoelectron spectroscopy (UPS).[3] However, each of these methods is subject to specific limitations or complications. For absorption measurements, values of effective masses and presumptions in the band structure (e.g., parabolic band) are needed to fit the energy dependence of the absorption coefficient near the absorption edge, which is also complicated by exciton effects.[4] PL and PLE are often subject to interference from competing processes such as strain splitting, phonon replicas, impurities, and other optical transitions in the constituent layers.[5] STM-based band gap measurements are often interfered by surface states existing on most semiconductor surfaces as well as artifacts such as tip induced band bending.[2] Thermionic emission requires current-voltage (I–V) measurements at different temperatures to extract the activation energies over barriers, and it does not work at low temperatures. It also requires separate C–V measurements to account for the modification of the effective barrier height due to Fermi level position in the doped layer and interface charges.[6] In C–V measurements, detailed device simulations are needed to consider the effect of deep levels in the barrier layer.[7] XPS and UPS can only probe the occupied electronic states and therefore are limited to measuring the valence band offsets.[3]

With a three-terminal extension of STM, ballistic electron emission microscopy (BEEM) and its associated spectroscopy (BEES) can independently control the kinetic energies of a "beam" of ballistic electrons or holes, and use it as an energetic probe to measure interfacial barrier heights, including Schottky barriers at metal-semiconductor (m-s) interfaces, and band offsets of shallow semiconductor HJs buried underneath a m-s interface.[8] An advantage of BEEM over STM is that tip induced band bending in the semiconductor substrate is eliminated, since the electric field in the tunnel gap is effectively screened by the metal base film. In previous BEEM/BEES measurements of band offsets, in order to measure the genuine barrier heights, a delta-doped layer below the single-barrier double HJs was inserted to reach a flat-band condition in the heterostructure. This could add ad-

 ©2010 The American Physical Society

ditional uncertainty due to the experimental error in the doping level.[9] To the best of our knowledge, most of the aforementioned methods, including BEEM/BEES, require separately designed n-type and p-type HJs to measure ΔE_C and ΔE_V independently, therefore the results are not necessarily self-consistent.

In this article, we illustrate that the band gap of a semiconductor material, as well as both the conduction band and the valence band offsets at a semiconductor HJ, can be measured simultaneously on the same device. In contrast to the traditional BEEM/BEES technique, which has unexceptionally relied on unipolar carrier transport, i.e., either electrons or holes are injected into an n-type or p-type Schottky contact respectively, our method utilizes both electron and hole injection into the same Schottky contact.[10] This enables simultaneous measurement of the energy maxima in both the conduction band and the valence band of the semiconductor collector. A summation of these two energy maxima gives the band-gap value of the corresponding constituent layer. An advantage of such bandgap measurement is that the same metal Fermi level at the m-s interface is used as the potential reference, therefore the measured band gap value is independent of the Fermi level pinning position. Another advantage is that it does not involve the generation and recombination of electron-hole pairs as in optical spectroscopies, so that it is free of exciton effects.

Some results of the present work have been briefly reported in a recent letter.[11] Here, we present more details on the physical principle, experimental techniques, data analysis, and additional results not included in Ref. 11. Some conclusions on the indirect-gap AlGaAs alloys in Ref. 11 have been changed after a careful reassessment of the experimental data. Special attention is given to those factors that crucially affect the accuracy of barrier heights determination such as barrier lowering effects. Our goal is to give a convincing exposition that such a method is suitable for measuring the electronic bandgap of a semiconductor as well as ΔE_C and ΔE_V of a HJ in a self-consistent manner.

In Sec. II, the methodology is outlined; in Sec. III, the experimental details including crystal growth, device fabrication, and tunnel junction and base-collector characteristics are presented; in Sec. IV, the details of direct and secondary ballistic carrier emission spectroscopy techniques are presented; in Sec. V, main results on the Al/GaAs/$Al_xGa_{1-x}As$ (100) system are given; in Sec. VI, sources of errors are discussed; and in Sec. VII, some conclusions are given.

II. METHODOLOGY

The concept of a Mott barrier,[12] in which an intermediate undoped i layer is located at the interface between a metal and a semiconductor, was applied to our sample design.[10] The benefit of using undoped i layer is to avoid doping induced band bending near the probed HJ. The bulk of the semiconductor is sufficiently heavily (degenerately) doped, so that the depletion width is determined by the i layer thickness and essentially does not vary under base-collector bias V_C. Mott barrier was one of the earliest cornerstones in the research regarding m-s contacts and has found practical ap-

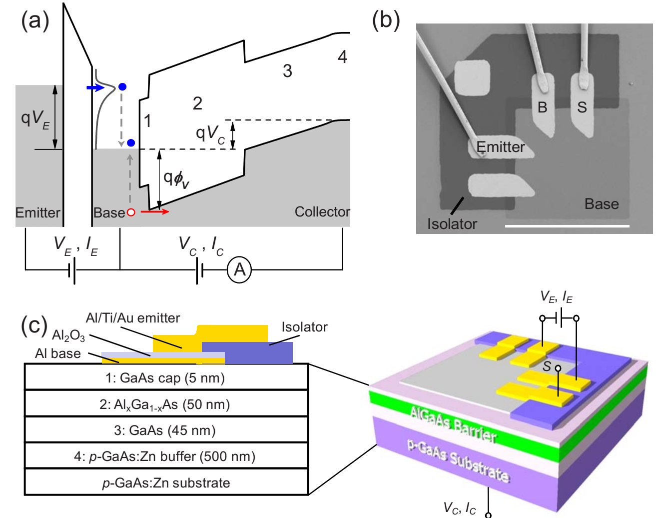

FIG. 1. (Color online) (a) Schematic energy diagram of a planar tunnel transistor with an undoped heterojunction collector grown on p-doped substrate. (b) Electron micrograph of a device (scale bar: 500 μm). (c) Schematic of the device structure and the collector layer sequence.

plications such as high-speed photodetectors. It is perceivable that a Mott barrier has a *linear* band profile in the depletion region and hence a constant electric field (E field) in the undoped layers, which can be tuned by V_C [see Fig. 1(a)]. Importantly, in a Mott barrier, a *nonequilibrium* flat-band condition in the depletion region near the m-s interface can be reached by applying appropriate V_C, accommodating precise measurement of HJ barrier heights without the need of introducing a delta-doping that may not be optimized.[9] In an earlier work, similar design principle was used to study the electroluminescence of self-assembled InGaAs quantum dots excited by ballistic electron injection.[10] In that work, a GaAs/$Al_{0.42}Ga_{0.58}As$ superlattice effectively acts as a current-blocking barrier layer, which suppresses the majority carrier (hole) drift-diffusion current when a forward bias is applied to the Schottky diode. This makes it possible to measure the tunnel injected ballistic electron current. Practically, it is still necessary to cool the device to low temperatures to further suppress the majority current contributed from thermal excitations, such as thermionic emission or thermally assisted tunneling across the valence-band barrier. Band gap of $Al_{0.42}Ga_{0.58}As$ was successfully measured with ~meV precision using ambipolar injection of ballistic electrons and holes, which has stimulated further investigations following this route, which has led to band offset measurements using a comparative method.[11]

III. EXPERIMENTAL

A. Crystal growth

Well-established ternary $Al_xGa_{1-x}As$ alloys (x=0.0 to 1.0) lattice matched to GaAs are considered one of the most matured III-V compounds in both epitaxial growth and characterizations, with well understood band structures as well as their interfacial properties with GaAs, therefore, they are

chosen as the model materials to validate our method. Lattice-matched GaAs/$Al_xGa_{1-x}As$ single-barrier (SB) double HJs were grown by molecular-beam epitaxy (MBE) in a Varian Gen II system on Zn-doped p-GaAs (100) substrates with miscut angle within 0.1°. The substrate Zn doping level is about 8×10^{18} cm^{-3}. The growth sequence started with a 500 nm heavily p-doped (5×10^{18} cm^{-3}) Be-:GaAs buffer layer [layer "4" in Fig. 1(a), and so forth]. The Be shutter was then closed to start the growth of the unintentionally doped layers composed of a 45 nm undoped GaAs (layer "3") followed by the 50 nm AlGaAs barrier (layer "2"). The AlGaAs barrier was capped with 5 nm undoped GaAs (layer "1") to prevent surface oxidation. It also establishes a potential reference as we will discuss in more details later. For a systematic study, samples with a wide range of Al mole fraction x=0.0, 0.1, 0.2, 0.3, 0.42, 0.6, 0.8, and 1.0, were grown under exactly the same condition. To check the effect of the GaAs caplayer thickness, a second set of samples with x=0.6, 0.8, and 1.0 were grown with slightly changed layer thicknesses of 40/50/10 nm for layer 3/2/1, so that the overall thickness of the undoped layers (100 nm) remains unchanged but the GaAs caplayer thickness is doubled from 5 to 10 nm. Unless stated explicitly, all the presented results refer to the first set of samples. The substrate temperature was 600 °C and the V/III ratio was 15 to 20. During the growth, the growth rate of GaAs was kept constant at 1.4 Å/sec and the growth rate of AlAs was tuned to obtain the desired Al mole fraction in AlGaAs. All the epitaxial structures are considered lattice matched ($\Delta a/a \leq 0.1\%$) to GaAs with slightly compressive strain. The error in Al composition is estimated to be ±0.01.

B. Device fabrication

Planar tunnel transistor represents a category of solid-state hot-carrier devices that was first proposed by Mead.[13] Historically it was also termed tunneling base transistor, metal-base transistor, or tunnel triode. In our tunnel transistor devices, thin-film Al/Al_2O_3/Al tunnel junctions are used as the hot carrier source and are fabricated using a shadow-mask technique.[14] Figure 1(b) and 1(c) show the details of the device structure. Non-alloyed Ti/Pt Ohmic contact to the p-GaAs substrate was made by blanket evaporation on the back surface after removal of native oxide. An 8 nm Al thin-film base Schottky contact with an area of 2.5×10^{-3} cm^2 (500×500 μm) was first evaporated on GaAs surfaces at pressures of low 10^{-7} Torr. The GaAs surfaces were treated in a 1:10 solution of $NH_4OH:H_2O$ for 60 s followed by a short deionized water rinse and nitrogen blow dry prior to Al evaporation. It is known that such chemical treatment forms a uniform interfacial native oxide layer on GaAs, which has minimal effect on BEEM measurements and improves the homogeneity of measured Schottky barrier heights.[15] The Al_2O_3 tunnel barrier was formed by ex situ ozone oxidation. An "L" shaped AlO_x isolator pad (70–120 nm thick), partially covering the oxidized Al base, was then deposited by e-beam evaporation of Al_2O_3 source. Here, x stands for slight deviations from stoichiometry due to oxygen loss. Nevertheless, the fabricated AlO_x films were found to be highly insulating. In contrast, SiO_x films evaporated from SiO_2 source showed much higher leakage current level due to the weaker Si-O bond, and therefore cannot be used. With typical leakage current level less than ~1 pA at 2 V, the AlO_x isolator pad insulates the emitter electrodes from contacting the semiconductor collector. The device was finalized by evaporating the Al/Ti/Au emitter stripes with thickness of 30/10/30 nm. The nominal tunnel junction area formed under each emitter stripe is approximately 5×10^{-5} cm^2. The Ti/Au metal overlayers were used to improve the wire bonding reliability.

Wire bonds to two of the Al stripes provide emitter and base contacts after one tunnel junction was shorted by carefully sourcing a current beyond the breakdown threshold of one Al_2O_3 tunnel barrier. The base contact resistance is typically $\sim10^1$ Ω after the tunnel junction is shorted. This contact resistance is composed of the resistance of the shorted Al_2O_3 barrier plus a small in-plane resistance of the Al base film and the resistance of external wiring. Although the base contact resistance is very small compared with the tunnel junction resistance (typically 10^1–10^2 kΩ at 1 V), it still acts effectively as a voltage divider to raise the actual base potential above ground level, and thus produces a small over-estimate in the measured barrier heights. To minimize such a systematic error, an extra base electrode [contact "S" in Fig. 1(b) and 1(c)] is connected to a sourcemeter sourcing zero current to monitor the actual base potential during the emitter bias sweep. The measured base voltage is typically less than ~10 mV in the entire range of the emitter bias used (up to 1.8 V). The BEES experiments were performed in a common-base configuration analogous to the Gummel plot in transistor terminology, by ramping up the emitter bias V_E (emitter-base tunnel junction voltage) from zero to positive or negative values at small voltage steps (e.g., 5 mV), and measuring the collector current I_C and emitter-base current I_E, while the collector bias, V_C, is kept at a constant. The emitter current I_E is recorded to calculate the common-base transfer ratio I_C/I_E. A series of BEES spectra are collected with a constant collector bias V_C spaced at a small interval (e.g., 0.05 or 0.1 V) to fine tune the E field in the depletion region. All the characterizations were performed at 4.2 K with the samples immersed in liquid helium to suppress the thermally excited currents such as thermionic emission and thermally assisted tunneling. The fabricated devices are robust against thermal cycles and reproducible results were acquired after the devices were left in ambient conditions for several months.

C. Tunnel junction characteristics

Ever since Al/Al_2O_3/Al tunnel junctions were first studied in early 1960s,[16] aluminum oxide films have been used extensively as tunnel barriers because of their specific physical properties. Amorphous Al_2O_3 has a large band gap (~7 eV), large barrier height for electron tunneling (~2 eV), high breakdown field (>10 MV/cm), low trap-assisted leakage, and excellent thermal and mechanical stability. Thin films of amorphous Al_2O_3 can be readily grown on top of Al metal by thermal oxidation in a controlled en-

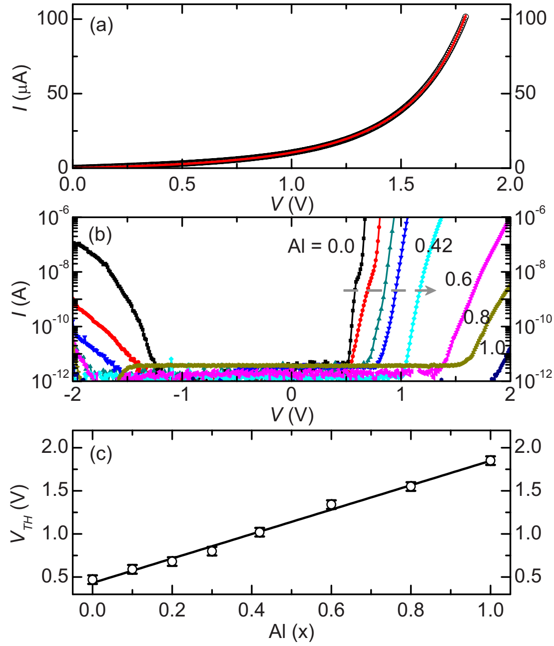

FIG. 2. (Color online) (a) Typical emitter-base tunnel junction I–V at 4.2 K. Red line is a fit by Simmons' equation. (b) Base-collector I–V curves for all the $GaAs/Al_xGa_{1-x}As$ (100) samples ($x=0.0-1.0$). (c) Measured collector current turn-on thresholds under forward bias (open circles) versus Al composition x. Solid line is a linear fit.

vironment using oxygen, oxygen plasma or ozone as oxidizers. The quality of thermal oxides is in general superior than those oxide films made by physical deposition (e.g., RF sputtering of Al_2O_3), the latter are often plagued by issues such as pinholes and poor adhesion.

The fabricated $Al/Al_2O_3/Al$ tunnel junctions exhibit hysteresis-free I–V characteristics [see Fig. 2(a)] at 4.2 K that are highly nonlinear and very reproducible. Only a slight decay in the tunnel current amplitude was observed after repetitive voltage stress. Their characteristics are examined by fitting the junction I–V curves with the Simmons' equation based on the Wentzel-Kramers-Brillouin (WKB) approximation.[17] The fit range for junction voltage is 0–1.7 V. The justification of using the WKB approximation for a trapezoidal barrier is given by the condition of $\Delta s\bar{\phi}^{1/2}>4$, where Δs is the distance between the barrier turning points in Å units and $\bar{\phi}$ is the mean barrier height in electron volts. Under such a condition, the WKB approximation gives the same functional form of tunnel probability as an exact method, except for a different pre-exponential factor.[18] This condition is validated in the case of Al/Al_2O_3 based tunnel junctions. It has been shown that in oxide tunnel junctions, fluctuations in the barrier thickness produce the so-called "hot spots" where local current density can be much higher, making the effective junction area just a small fraction of the nominal junction area.[19,20] Therefore, in the fittings we left the barrier height φ_0, the oxide thickness s, and effective junction area A as free parameters. The dielectric constant κ of Al_2O_3, which accounts for the image force modification of the oxide barrier, is taken as 9.0 as a median value of numbers cited in most publications (7–10). Typical values of the calculated fit parameters are $\varphi_0\sim 1.7$ V, $s\sim 10$ Å, and $A\sim 10^{-11}-10^{-9}$ cm^2. These values qualitatively agree with reported values for thermally grown aluminum oxides.[21,22] The effective junction area may be underestimated due to the prefactor of the WKB approximation. The observed breakdown voltage of our tunnel junctions is in the range of 1.8–2.3 eV, which is translated to a breakdown field of $\sim$20 MV/cm if using the fitted oxide thickness. It is notable that experimentally both the barrier height and dielectric constant of thin-film Al_2O_3 are not well defined properties and may vary with the film thickness,[23] therefore fitting tunnel junction I–V curves at fixed temperature itself is not sufficient to determine these material parameters exclusively. However, more detailed study of Al_2O_3-based tunnel junctions are beyond the scope of this work.

D. Base-collector characteristics

Prior to BEES experiment, the two-terminal I–V characteristics across the base-collector contacts are first examined. The purpose is to establish the maximal range of V_C allowed in the BEES measurement beyond which the internal majority current starts to overwhelm the externally injected ballistic current. Figure 2(b) summarizes typical base-collector I–V characteristics for $GaAs/Al_xGa_{1-x}As$ (100) samples measured at 4.2 K. Most of the tested devices show a highly asymmetric rectifying lineshape. Under reverse bias up to −1.5 V, current is essentially zero, i.e., in the sub-pA level from the noise floor of electronics. Under forward bias, I_C remains miniscule until V_C reaches a threshold value, beyond which current rises in an exponential fashion. The turn-on threshold V_{TH} is in the range of 0.5–1.85 V and varies slightly across devices. As shown in Fig. 2(c), it increases linearly with the Al composition x as $V_{TH}=0.43+1.42x$ (V) ($\pm 5\%$), suggesting that the forward current mechanism is probably field emission over the valence-band barrier at the bottom GaAs/AlGaAs HJ under high enough E field. At 4.2 K, most of the thermally activated currents should be frozen out, small fluctuations in the turn-on thresholds ($\sim$0.1 V) across different devices may be related to defect mediated leakage mechanisms. For most devices, the window of V_C with negligible internal current is sufficiently wide to allow both electron and hole ballistic currents to be measured. An exception was found for Al $x=0.0$ sample (GaAs), in which ballistic electron current under forward bias cannot be measured due to the overwhelming internal hole current.

IV. BALLISTIC CARRIER EMISSION SPECTROSCOPY

A. Direct BEES(BHES)

In a conventional BEEM device with unbiased collector, the E-field in the collector depletion region is predetermined by the doping profile. Consequently, the species of ballistic carriers collected is restricted to majority carriers, which can only probe the corresponding band, i.e., ΔE_C for an n-type collector or ΔE_V for a p-type collector. Such restriction is lifted in our case. Using a tunnel triode configuration and a tunable E-field in the depletion region, it is made possible to

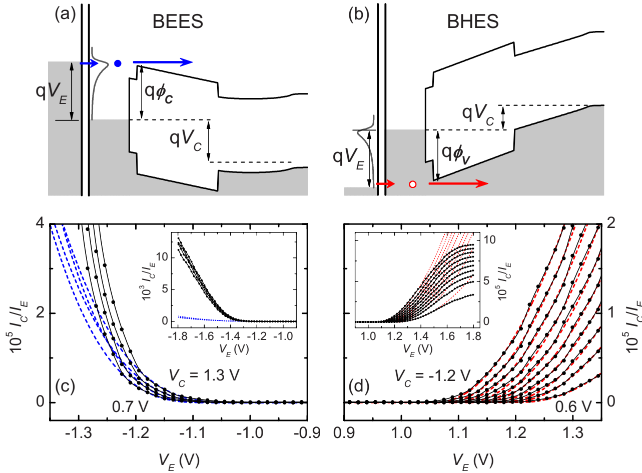

FIG. 3. (Color online) Ballistic electron(hole) spectra on a $GaAs/Al_{0.8}Ga_{0.2}As$ (100) sample plotted as (I_C/I_E) vs negative (c) and positive (d) V_E, measured at fixed V_C. The spectra are spaced at 0.2 V V_C intervals for clarity. Dashed lines are power-law fits for a superthreshold range of 0.2 V. Insets show the complete spectra. Corresponding ballistic carrier injections are shown in (a) and (b), respectively.

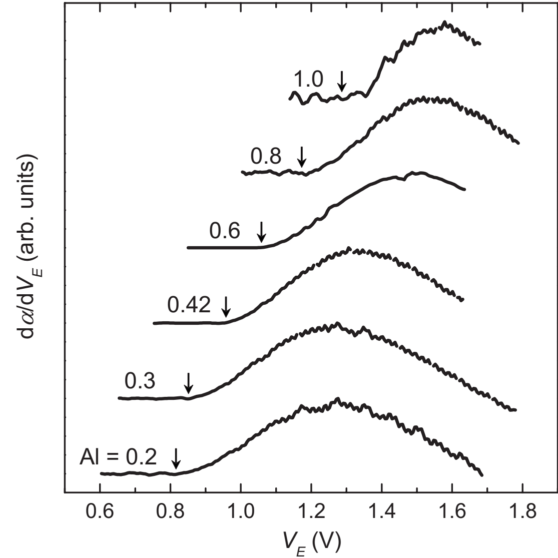

FIG. 4. Derivative ballistic hole spectra on $GaAs/Al_xGa_{1-x}As$ (100) samples (x=0.2–1.0), measured at V_C=0.7 (except for x =0.6 sample measured at 0.5 V). The spectra are normalized and vertically shifted for clarity. Arrows mark the valence-band barrier heights ϕ_V.

obtain *ambipolar* carrier injection into the same collector heterostructure, utilizing all possible mechanisms including both direct ballistic electron(hole) emission, BEES(BHES), and secondary ballistic electron(hole) emission, s-BEES(s-BHES). Such processes are illustrated by the schematic band diagrams in Figs. 3 and 5, respectively. Ballistic carrier injections by direct BEES(BHES) process are conceptually straightforward and have been covered in a few review articles.[8] Therefore we will only give a brief discussion here. Figures 3(a) and 3(b) highlight a prerequisite for such direct injection processes to occur, i.e., the E field in the i layer needs to be in the correct direction to favor the collection of tunnel injected ballistic carriers. Figures 3(c) and 3(d) plot a series of BEES(BHES) spectra measured under a constant collector bias. The collection efficiency, or the amplitude of I_C, increases with the E-field strength in the depletion region. Similar behavior was observed in BEEM studies of reverse-biased Schottky diodes, which can be explained as a reduction of the energy-dependent backscattering of electrons in the depletion region by the stronger E field. Such electron backscatterings into the metal were mainly attributed to the interactions with phonons inside the depletion region near the m-s interface.[24]

The direct BEES(BHES) spectra were fitted with the prevailing Bell-Kaiser (B-K) theory, in the form of a power-law function $\alpha \propto (V_E - \phi_{C(V)})^\gamma$ in the near-threshold regime. The optimal fit range determined by computing χ^2 was found to be ~200 meV. We found that most of the BHES spectra can be well fitted with a square law γ=2–2.5, while for most of the BEES spectra a larger power-law exponent $\gamma \geq 3$ is needed to obtain reasonable fit. At higher emitter bias, the measured ballistic electron current is always larger than the power-law fit for the near-threshold regime. This is probably due to the contribution from higher-lying transport valleys, e.g., Γ band for the case of Al $x > 0.42$. Opposite case occurs for the measured ballistic hole current, which falls below the power-law fit at higher bias and gradually levels off. In some cases, hole current even starts to decrease with bias. We noticed that it is also feasible to fit the BEES(BHES) data with a multivalley B-K model incorporating *a priori* $Al_xGa_{1-x}As$ band structures (e.g., effective masses and nonparabolicity). However, we did not perform such fitting procedures since they may not be generally applicable for less-known materials.

The collection efficiency for ballistic holes is much lower than that for electrons, typical transfer ratio for holes is ~0.01% vs. ~1% for electrons at 1.8 V. This is partially attributed to the shorter attenuation lengths for hot holes. In Al films, the measured attenuation length for ~1 eV holes is less than 50 Å,[25] compared with a value of ~150 Å for 2 eV electrons.[26] At higher bias, the spectral shape for ballistic holes is different than that of electrons. This phenomenon was attributed to the reversed energy distribution of the ballistic holes, which also accounts for a much lower injection efficiency. The peak tunneling probability is always close to the Fermi level of the source electrode. For electron injection, most of the collected electrons originate from the top of the tunnel distribution near its maximum [Fig. 3(a)]. For hole injection, most of the collected holes originate from the low-energy tail of the tunnel distribution [Fig. 3(b)]. As a result, the number of electrons created per unit energy remains nearly constant with bias, whereas the number of holes created per unit energy decreases with increasing bias.[27] More details of the ballistic hole spectra are revealed by calculating their first derivatives. Figure 4 shows the derivative BHES spectra for Al x=0.2–1.0 samples calculated after smoothing the raw data by averaging five adjacent data points. Several prominent features are identified from the derivative spectra. The onsets in the derivative spectra agree with the current turn-on thresholds determined by the square-

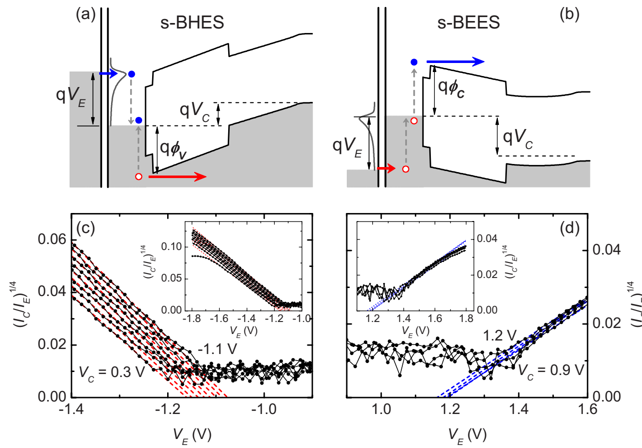

FIG. 5. (Color online) Secondary ballistic hole (electron) spectra on a GaAs/$Al_{0.8}Ga_{0.2}As$ (100) sample plotted as $(I_C/I_E)^{1/4}$ vs negative (c) and positive (d) V_E, measured at fixed V_C. The spectra are spaced at 0.2(0.1) V V_C intervals for clarity. Dashed lines are linear fits for a superthreshold range of 0.2 V. Insets show the complete spectra. Corresponding Auger-like secondary ballistic carrier injections are shown in (a) and (b), respectively.

law fit. Above the onset, the derivative first increases linearly with the bias and then roll off to a maximum value. The energy separation between the maximum and the onset of the derivative is ~400 meV, which remains nearly a constant for all the Al compositions. As the bias further increases, the derivative decreases in a linear manner, and may even enter a negative differential transconductance (NDTC) regime for some samples. The roll-off of ballistic hole spectra was observed previously in Au/*p*-GaAs(100) Schottky diodes, which can be fitted with the B-K model assuming interface transverse momentum conservation and two valence bands (the light- and heavy-hole bands).[27] However, for the binary GaAs, the 0.34 eV energy separation between the spin-orbit splitoff band and the degenerate light- and heavy-hole bands is very close to the maximum of the experimental derivative spectra, making such factor difficult to be excluded. For the ternary $Al_xGa_{1-x}As$ alloy, the splitoff band energy should decrease with the Al composition,[28] which disagree with the nearly constant energy separation observed on samples with different Al composition, therefore we can safely exclude the effect of splitoff band.

B. Secondary BEES(BHES)

To study subsurface barrier heights, s-BEES(s-BHES) process, also termed reverse or scattering BEES(BHES) mode, can also be utilized. Figure 5(a) illustrates an example for s-BHES process, i.e., hot electrons tunnel into the base from a negatively-biased emitter with the *p*-type collector unbiased or in reverse bias. The repulsive *E*-field in the conduction band prevents hot electrons from being collected across the m-s interface into the *p*-type substrate. Rather, they lose their kinetic energies via inelastic scattering events in the metal base. Due to the large number of available electron states below the Fermi level, the dominant inelastic scattering mechanism for hot electrons is electron-electron (*e*-*e*) scattering, which generates electron-hole pairs in a mechanism analogous to Auger process. Such *e*-*e* scatterings are very efficient in thermalizing the hot-electron distribution. As a result, a distribution of hot holes are produced and some of them may ballistically traverse the base and be transmitted into the valence band of the collector. These hot holes can be used as an energetic probe to sense the valence-band barrier height ϕ_V. As we have discussed earlier [see Fig. 3(a)], without reversing the emitter bias polarity, one can reverse the *E*-field direction in the *i* layer by applying a forward collector bias beyond the flat-band condition, so that hot electrons are injected into the conduction band by direct BEES process to probe the conduction-band barrier height ϕ_C. Similar physical mechanisms apply for positive emitter biases [see Figs. 5(b) and 3(b)] The bandgap value of the barrier material can therefore be possibly determined by summing these two barriers ϕ_V and ϕ_C.

As a two-step scattering process, the collector transfer ratio $\alpha \equiv I_C/I_E$ for s-BEES (s-BHES) is much smaller than that its direct counterpart, typically just a few percent of the latter. If sorted by magnitude, $\alpha_{\text{BEES}} \gg \alpha_{\text{s-BHES}} \gg \alpha_{\text{BHES}} \gg \alpha_{\text{s-BEES}}$. The lower collection efficiency for secondary carriers can be explained by the rule of transverse momentum conservation at the m-s interface. The momentum distribution of secondary carriers in *k* space are more isotropic if compared with the highly forward-directed primary carriers.[29] Consequently most of the secondary carriers impinging the m-s interface are directed outside the acception cone which is determined by the effective mass mismatch and the barrier height. Nonetheless, we found that the energy resolution of experimental s-BEES (s-BHES) spectra is not deteriorated. In fact, with appropriate fitting procedures, the standard deviations in fitting the s-BEES spectra are even smaller than the values for BEES spectra from power-law fit. Intuitively, one may attribute this resolution improvement to the quartic spectral shape of the Auger-like process.[30] For s-BEES (s-BHES), in the near-threshold regime $\alpha \propto (V_E - \phi_{C(V)})^4$, in contrast to a square law $\alpha \propto (V_E - \phi_{C(V)})^{2-2.5}$ for direct BEES (BHES) (the power-law exponent differs from 2 in the B-K model to 2.5 in the Ludeke-Prietsch model).[8]

As seen in Figs. 5(c) and 5(d), the spectral shapes of $\alpha^{1/4}$ for both s-BEES and s-BHES are indeed linear in the near-threshold regime. For secondary holes, the bias range in which the linear dependence holds can be larger than 400 meV, due to the relative simple valence-band structure. A least-squares linear fit of $\alpha^{1/4} = \alpha_0(V_E - \phi_{C(V)})$, which includes only two free parameters, gives $\phi_{C(V)}$ with a typical standard deviation 1–2 meV at 4.2 K ($k_B T \sim 0.4$ meV). In comparison, fitting a BEES spectra with similar signal-to-noise ratios by a multivalley B-K model gives a standard deviation in the order of 10 meV. Actually, the difference in the power-law exponent itself is not sufficient to account for the improved fitting results. It is more likely a result of minimized number of fitting parameters and the linearization scheme we applied, rather than the difference in spectral shape. As a support, we found that the standard deviation can be greatly reduced if the BEES spectra were first linearized in the form of $\alpha^{1/\gamma} = \alpha_0(V_E - \phi_{C(V)})$ near the threshold regime. It was found that the optimal values of γ after minimizing χ^2 are usually greater than 2, in line with the observation in

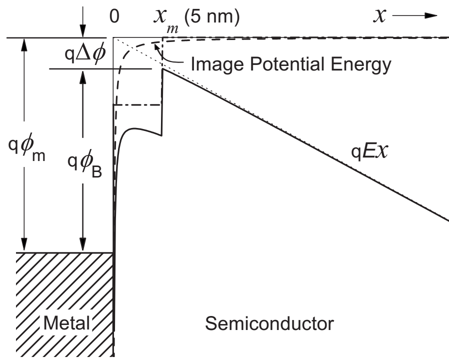

FIG. 6. Energy-band diagram between a metal and an undoped semiconductor heterostructure. The "ideal" Schottky barrier $q\phi_m$ at flat-band condition is reduced to the effective barrier $q\phi_B$ when an E-field exists in the semiconductor. Solid line shows the total potential profile with the image potential included. Image potential energy is calculated using a permittivity $\kappa_S=3$. E-field strength is 2.5×10^5 V/cm.

power-law fits. It is worth noting that such a phenomenological fitting process does not require *a priori* band parameters, e.g., effective masses, making the present method model independent and applicable to materials for which such knowledge is not reliably available.

In practice, the apparent turn-on thresholds of $\alpha^{1/4}$ in an experimental s-BEES (s-BHES) spectrum, if defined by the inflection point of the curve, are always larger than the values from a linear fitting, i.e., intersection of x axis. Keep in mind that the apparent inflection point in an experimental s-BEES spectrum is caused by the noise floor of the electronics. In our setup, typical background noise level of I_C is in the order of 0.1 pA, if divided by $I_E\sim10$ μA at $V_E=1$ V, it produces a background level $\alpha_{bg}\approx1\times10^{-8}$ and correspondingly $\alpha_{bg}^{1/4}\approx0.01$. Therefore, the intersection of x axis should always be used when trying to determine the turn-on thresholds in a s-BEES (s-BHES) spectrum.

C. Barrier lowering effects

In general, one needs to take caution in interpreting the apparent barrier heights measured in BEES measurements, since they are susceptible to various barrier lowering effects. One of the implications of Mott barrier is the functional dependence of the barrier lowering on the applied bias. The familiar form of image-force barrier lowering $\Delta\phi\propto V_C^{1/4}$ for a uniformly doped Schottky barrier[31] changes to $\Delta\phi\propto V_C^{1/2}$ for an undoped Mott barrier. Such image-force lowering effect dominates for reverse bias regime, as supported by BEEM characteristics of reverse-biased Au/Si Schottky diodes.[24]

In forward bias regime, which is the relevant case here to measure barriers near the flat-band condition, the image-force contribution is negligible if compared with the contribution from the E-field in the i layer. This is illustrated by the generic band diagram in Fig. 6. Assuming an image-force permittivity $\kappa_S=3$, which is much smaller than the static permittivity of GaAs (12.9), the calculated image potential energy, $q^2/16\pi\kappa_S\epsilon_0 x$, is still negligible at the GaAs/AlGaAs HJ ($x_m=5$ nm) when compared with the E-field effect at a field strength $E=2.5\times10^5$ V/cm. κ_S is expected to be smaller than the static value, since it is possible that the electron transit time from the m-s interface to the barrier maximum x_m is shorter than the dielectric relaxation time. However, it has been known that the image-force permittivity of GaAs is approximately the same as the corresponding static value.[32] If a static permittivity $\kappa_S=12.9$ is used, the image force lowering at x_m is about 5 meV, which is only 10% of the E-field effect at a field strength of 1×10^5 V/cm. Therefore we can henceforth safely overlook the image-force effect and just consider the E-field induced barrier lowering. For a degenerately doped substrate, the depletion width is essentially a constant, and the E-field contribution can be estimated by the sample geometry as

$$\Delta\phi=(x_m/D)(V_C-V_{\mathrm{FB}}), \quad (1)$$

here $D=100$ nm is the overall thickness of the i layer. It predicts a slope of barrier height lowering versus the collector bias ~50 meV/V, which is determined by the sample structure rather than the dielectric response in typical image-force effect. This slope is very close to the observed values in both GaAs/AlGaAs and GaAs/AlGaInP systems.[11] As a support, in the second set of GaAs/$Al_{1-x}Ga_xAs$ samples ($x=0.6,0.8,1.0$) with the same 100 nm i layer thickness but the GaAs cap thickness increased to 10 nm, the slope of barrier height lowering is found to be nearly doubled to ~110 meV/V.[33] Note that the degenerate doping in the p-substrate is necessary to prevent carrier freeze-out at 4.2 K. With a partial carrier freeze-out, the depletion width would increase substantially and greatly reduce the slope of barrier height lowering.

From the above analysis, it is clear that the measured apparent barrier heights are subject to the barrier lowering effects, which is mainly determined by the E-field in the undoped layers. To obtain the genuine barrier heights, a series of collector-current spectra are measured under constant collector biases spaced at small (0.05–0.1 V) intervals for each emitter bias polarity. A complete survey of ballistic carrier injection is therefore mapped out combining two adjustable parameters, V_C and V_E. As seen previously, e.g., Figures 5(c) and 5(d), the measured barrier heights indeed show redshifts with the collector bias. In our experiments, no separate C–V measurement is needed to determine the flat-band condition. Instead, it is determined by the criteria that the polarity of I_C immediately following its turn-on threshold is reversed, indicating a transition from electron to hole injection (represented by e→h hereafter, and vice versa) occurs. Values of ϕ_V and ϕ_C near the flat-band condition are used to calculate the values of E_g and band offsets.

Figure 7 summarizes the near-threshold regions of collector-current spectra for all the GaAs/AlGaAs samples measured under negative V_E sweep, so that electrons are tunneled into the metal base. It clearly shows that if the applied V_C exceeds a critical sample-specific value, the species of collected carriers reverses from hole to electron, i.e., the polarity of superthreshold I_C changes from negative to positive. This corresponds to a crossover from s-BHES to BEES process. As V_C getting close to but not yet reaching the critical value, although holes are first injected into the collector,

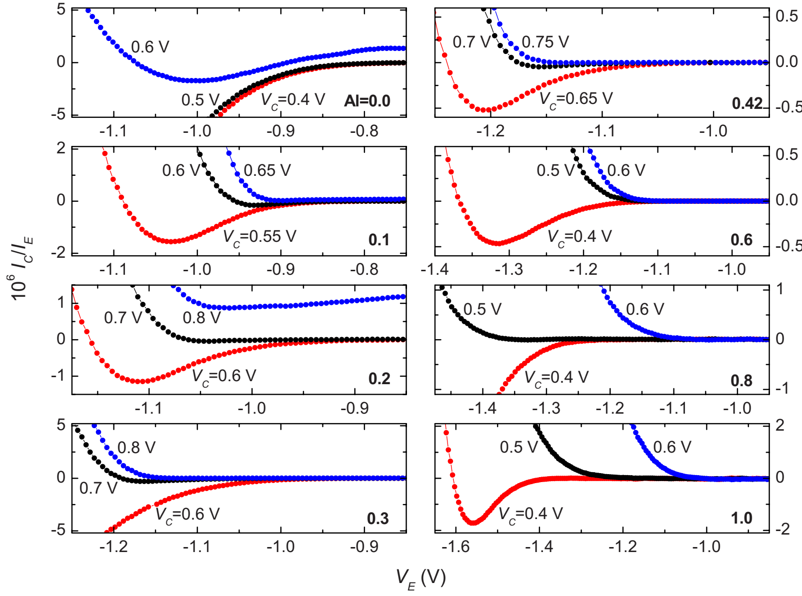

FIG. 7. (Color online) Near-threshold regions of collector-current spectra for all the GaAs/AlGaAs samples measured under negative V_E and $V_C \approx V_{\mathrm{FB}}$ showing the transition from hole injection ($I_C<0$) to electron injection ($I_C>0$).

electron injection may emerge under high-enough V_E, which is manifested by the upward turn of the curve that eventually drive the net current into the positive zone.

D. Flat-band voltage

It has been shown that the electrostatic potential profile for a Mott barrier can be calculated by solving the Poisson equation analytically.[34] The flat-band voltage V_{FB} corresponds to the forward bias beyond which there arises a local potential maximum within the *i* layer due to the space charge of carriers. For *p*-doped substrate, V_{FB} is given as

$$V_{\mathrm{FB}} = \phi_B + (kT/q)ln[\pi^2 N_A/2N_V(D/r_d)^2], \qquad (2)$$

where ϕ_B is the Schottky barrier height; N_A is the acceptor concentration in *p*-doped substrate; $N_V=2(m_v kT/2\pi\hbar^2)^{3/2}$ is the effective density of states in the valence band (m_v is the density-of-states effective mass for holes); $r_d = \sqrt{\kappa\epsilon_0 kT/q^2 N_A}$ is the Debye length; while the rest of the symbols have their usual meanings. This formula gives an approximately linear temperature dependence of V_{FB}, except for low temperature regime ($T<100$ K) where V_{FB} starts to level off. It also predicts that as temperature approaches zero, V_{FB} asymptotically approaches ϕ_B. Applying experimental parameters in our case ($N_A=5\times10^{18}$ cm^{-3}, $\phi_B=0.708$ V, $D=100$ nm, $m_v=0.45m_0$, $\kappa=12.9$), the estimated values of V_{FB} are 0.53 V at 300 K, and 0.7 V at 4.2 K. In the above estimation, the temperature dependence of the Schottky barrier height has been neglected.

Figure 8 summarizes the V_C dependence of measured ϕ_V and ϕ_C for all the GaAs/AlGaAs samples. The slopes for barrier heights, especially for ϕ_V, are close to the expected value of 50 mV/V (dashed lines). Overall, the estimated $V_{\mathrm{FB}}\approx 0.7$ V is close to the observed V_C values near which the polarity of collector current is reversed immediately following its turn-on threshold, indicating a transition of h→e, or vice versa. In the direct-gap regime ($x\leq 0.42$), the h→e transition occurs at $V_C=0.6-0.7$ V when a negative emitter bias was used. However, no h→e transition followed by s-BEES process was observed under positive emitter bias. Therefore ϕ_C was determined by the direct BEES spectra. The missing of electron injection in a s-BEES process for direct-gap samples may be related to the *k*-distribution of secondary electrons and momentum filtering at the GaAs/AlGaAs interface, which will be discussed in more details later. More intriguing phenomena occur in the indirect-gap regime ($x>0.42$), where the h→e transition occurs at different V_C if the emitter bias polarity were reversed. For $-V_E$ sweep it occurs at $V_C\approx 0.5$ V, while for $+V_E$ sweep it occurs at $V_C\approx 0.8$ V. The 0.3 V split of the apparent V_{FB} under different V_E polarity is probably a consequence of the asymmetry between electron and hole tunnel distributions, which

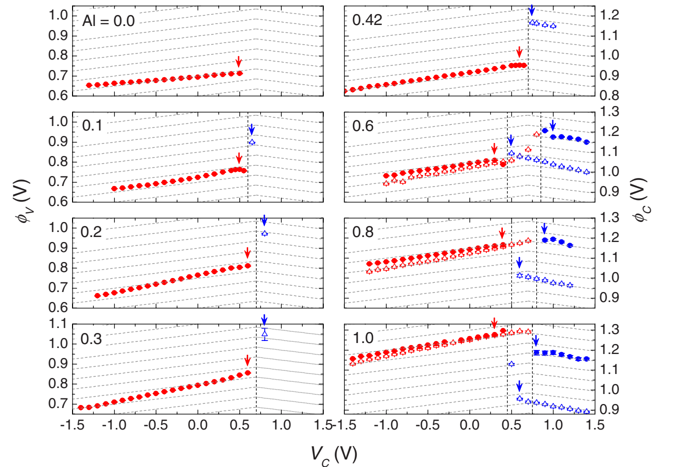

FIG. 8. (Color online) V_C dependence of conduction- and valence-band barrier heights ϕ_C (blue) and ϕ_V (red) for all the GaAs/AlGaAs samples measured by the direct (open triangles) and secondary (solid circles) ballistic emissions. Slant lines highlight the expected slope of 50 meV/V for barrier lowering by *E*-field effect. Vertical lines show the values of V_C near which the h→e transitions occur. Arrows mark the values of genuine barrier heights used to determine the bandgaps and band offsets.

TABLE I. Barrier heights of $Al/GaAs/Al_xGa_{1-x}As$ (100) at 4.2 K

Mole fraction x	ϕ_V (eV)	$\phi_C^{-/+}$ [a] (eV)	ΔE_V (eV)	$\Delta E_C^{-/+}$ (eV)	$E_g^{-/+}$ (eV)	E_g from Ref. 35
0.0	0.708(1)[b]					1.519(Γ)
0.1	0.764(2)	0.900(1)	0.055(2)	0.089(1)	1.664(3)	1.677(Γ)
0.2	0.815(2)	0.972(2)	0.106(2)	0.162(2)	1.787(4)	1.813(Γ)
0.3	0.855(1)	1.063(2)	0.147(1)	0.252(2)	1.918(3)	1.937(Γ)
0.42	0.958(1)	1.165(1)	0.249(1)	0.354(1)	2.124(2)	2.086(Γ)
0.6	1.053(1)	1.103(1)/1.181(2)	0.344(1)	0.292(1)/0.370(2)	2.155(2)/2.233(3)	2.123(X)/2.202(L)
0.8	1.164(1)	1.016(3)/1.185(2)	0.449(1)	0.205(3)/0.374(2)	2.181(4)/2.349(3)	2.179(X)/2.331(L)
1.0	1.277(2)	0.957(2)/1.186(12)	0.569(2)	0.146(2)/0.375(12)	2.234(4)/2.463(14)	2.240(X)/2.460(L)

[a] −/+ represents values measured by $-/+V_E$ sweeps.
[b] Values in parentheses are standard deviations in meV.

makes s-BEES process the least-efficient injection mechanism. Values of ϕ_V measured by s-BHES and BHES processes are closely matched, while for ϕ_C a large discrepancy up to ~200 meV was observed under different V_E polarity. In our previous letter,[11] such a discrepancy was neglected since only the s-BEES data were used to determine ϕ_C values for the indirect-gap samples. As we will present in the results section, it turned out that ϕ_C values obtained from the direct and secondary BEES processes correspond to the X- and L-conduction band valleys, respectively.

V. RESULTS AND DISCUSSION

The main results from the ternary AlGaAs alloy system are summarized in Table I and plotted in Fig. 9. In Table I, −/+ represents values measured by $-/+V_E$ sweeps. The measured barrier heights ϕ_V and ϕ_C of $Al-Al_xGa_{1-x}As$ Schottky contacts, as functions of Al composition x, are shown in Figs. 9(b) and 9(c), respectively. ϕ_V increases linearly with x in the full range of Al composition ($0<x<1$). A least-squares linear fit gives $\phi_V=(0.703\pm0.008)+(0.578\pm0.015)x$ (V). This linear trend is expected, since all the valence-band maxima (heavy hole, light hole, and splitoff bands) of AlGaAs are located in the vicinity of the Brillion zone center. The measured ϕ_C, however, shows a sharp change of slope at $x=0.42$ as a result of the direct-indirect transition. In the direct-gap regime ($x\leq0.42$), a linear fit gives $\phi_C=(0.815\pm0.005)+(0.831\pm0.015)x$ (V); while in the indirect-gap regime ($x>0.42$), a linear fit gives $\phi_C^+=(1.143\pm0.006)+(0.054\pm0.011)x$ (V) for the L band and $\phi_C^-=(1.318\pm0.007)-(0.362\pm0.012)x$ (V) for the X band.

Values of band offsets are obtained with a *comparative* method. The valence band offset $\Delta E_V(x)$ of $GaAs/Al_xGa_{1-x}As$ is obtained by

$$\Delta E_V(x) = \phi_V(x) - \phi_V(0), \tag{3}$$

where $\phi_V(0)$ is the measured value for GaAs. Here, it is assumed that the Fermi level pinning position at the m-s interface with regard to the vacuum level remains unchanged for devices with different Al mole fraction. This assumption is considered reasonable, given the facts that the same GaAs cap layer was used for all the samples, and the same chemical treatment was applied prior to Al base deposition. It is further validated by the fact that the measured ϕ_V shows a nearly perfect linear dependence on x. A least-squares linear fitting gives $\Delta E_V(x)=(0.578\pm0.015)x$ (eV), with a negligible intercept of -6 ± 8 meV at $x=0$. This slope is slightly higher than the consensus value of 0.51,[28] but is very close to the result of 0.55 obtained from thermionic emission current over p-type barriers.[6]

The conduction band offset $\Delta E_C(x)$ of $GaAs/Al_xGa_{1-x}As$ is derived from

$$\Delta E_C(x) = \phi_C(x) - E_g(0) + \phi_V(0) = [E_g(x) - E_g(0)] - \Delta E_V(x) \tag{4}$$

where $E_g(0)$ is the bandgap of GaAs (taken as 1.519 eV at 4.2 K[35]). The derived $\Delta E_C(x)$ increases linearly with x in the direct regime (Γ band). $\Delta E_C(x)=(0.831\pm0.015)x$ (eV) for $x\leq0.42$, with a negligible intercept of 4 ± 4 meV at $x=0$. A direct-indirect transition of the conduction band minima at $x=0.42$ is indicated by the abrupt slope change at this composition. The deduced direct-gap Γ band offset ratio $r\equiv\Delta E_C/\Delta E_V$ is found to be 59:41 (±3%), which is very close to the consensus value of 60:40 (the so-called 60:40 rule).[28] Previously, conduction band offsets at direct-gap $Au/GaAs/Al_xGa_{1-x}As$ (100) interfaces ($x\leq0.42$) in delta-doped SB HJs were measured by BEEM experiments down to 77 K.[9,40] It was found that the collector current fitted by a multivalley B-K model is dominated by AlGaAs Γ and L channels, and the contribution from the off-axis L channel is even larger due to interfacial scatterings at the m-s interface that can redistribute the injected electron flux.[39] However, valence band offset of the same structure could not be measured in such traditional BEEM experiments.

In the indirect-gap regime, the L band offset $\Delta E_C^+(x)$ increases at a smaller slope with x, which is $E_C^+(x)=(0.332\pm0.006)+(0.054\pm0.011)x$ (eV) for $x>0.42$ by a linear fit. The less ideal R^2 in the fitting result suggests that some band bowing effect may exist in the indirect-gap regime. In contrast, the X band offset $\Delta E_C^-(x)$ decreases with x, which is $E_C^-(x)=(0.507\pm0.007)-(0.363\pm0.012)x$ (eV) for $x>0.42$ by a linear fit. The limited number of available data

points prevents us from making a conclusive remark on the band bowing for X band.

It is found that for the binary GaAs sample ($x=0$), although ϕ_V can be readily measured both by BHES and s-BHES processes, ϕ_C cannot be measured due to the overwhelming internal hole current under the forward collector bias needed for ballistic electron injection. As a result, only $Al_xGa_{1-x}As$ band gap values for $x \geq 0.1$ can be obtained.[36] In our previous letter, ϕ_C of the $x=0.1$ sample was also reported as unmeasurable.[11] However, a reexamination of the data found that ϕ_C can be obtained by fitting the spectrum at $V_C=0.65$ V, where the internal current background is not yet dominating. We have included the values for $x=0.1$ and revised the fit parameters accordingly in the present paper. The changes in the fit parameters are found to be negligibly small to affect the main conclusions made in our previous letter.

The measured band gaps of $Al_xGa_{1-x}As$, after summing ϕ_V and ϕ_C [Table I and Fig. 9(a)], agree well with the established data acquired by optical methods[35] (within 2%). In the direct-gap regime, no perceivable band bowing effect was observed, which is in line with a few optical studies.[37,38] Note that in theoretical treatments, a quadratic or even cubic band bowing for the AlGaAs alloy was often assumed,[35] somehow we do not intend to make any conclusion on the band bowing effect due to limited data points.

In the indirect-gap regime, a rather surprising observation is the selective collection of ballistic electrons into the X or L channels of the AlGaAs conduction band respectively by the direct or secondary emission processes. Previous BEEM experiments on indirect-gap $Au/GaAs/Al_xGa_{1-x}As$ (100) ($x=0.7, 1.0$) found the lowest threshold in BEEM current to be the $Al_xGa_{1-x}As$ X band,[9] which is in line with our observation from the direct BEES data. In the literature, electron transport over the indirect-gap GaAs/AlGaAs barrier has been largely attributed to the X channel.[41] To the best of our knowledge, there has been no conclusive report of L channel transport by either traditional methods such as thermionic emission or BEEM experiments. This perhaps can be explained by the fact that the s-BEES process has been relatively less explored. The observation of X electrons in the indirect-gap regime ruled out our previous conjecture that their contribution was attenuated by bulk scatterings due to their much shorter mean free path.[11] To reinforce the argument that interfacial processes rather than bulk scattering rates matter, consistent results on both the X- and L-valley conduction band minima were found for the second set of samples with 10 nm GaAs caplayer thickness (data not presented).[33]

The observed selective coupling of electrons generated by direct(secondary) ballistic emission into the X(L) valley of indirect-gap $Al_xGa_{1-x}As$ alloys can be interpreted in the framework of parallel momentum conservation. It is established that close lattice matching between Al and GaAs gives rise to quasiepitaxial Al/GaAs (100) interface.[42] Even for our evaporated polycrystalline Al films, local domains with good atomic registry may form at the Al/GaAs interface. As a result of the translational symmetry, the electron momentum component parallel to the substrate plane $k_{\parallel}$ may be better conserved across the Al/GaAs interface than the case of Au/GaAs, causing a much stronger momentum filtering effect. In

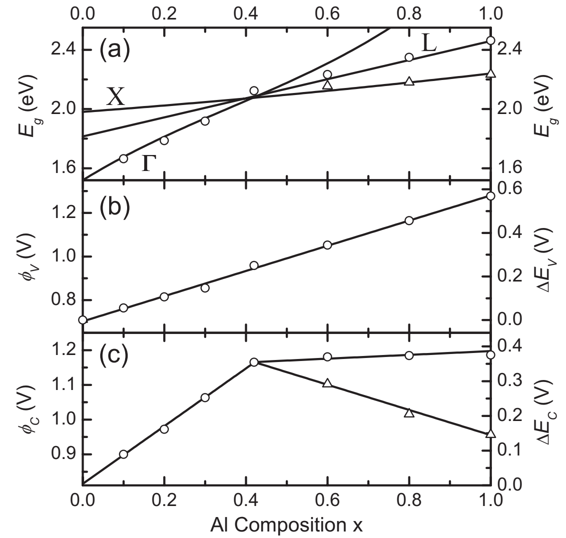

FIG. 9. Measured Al mole fraction x dependence of (a) energy bandgap of $Al_xGa_{1-x}As$ (solid lines are from Ref. 35), (b) valence-band barrier ϕ_V and valence-band offset of $GaAs/Al_xGa_{1-x}As$ (solid line is a linear fit), and (c) conduction-band barrier ϕ_C and conduction-band offset of $GaAs/Al_xGa_{1-x}As$ (solid lines are linear fits). All the data are taken at 4.2 K. Triangles are data points for the indirect X band.

direct BEES, most of the incoming electrons have a large perpendicular momentum $k_{\perp}$ pointing into the substrate, so that they can easily couple into the available states in conduction bands near the Brillouin zone (BZ) center. For indirect-gap AlGaAs, the one out of the six X band minima which is projected to the BZ center becomes the most probable transport channel. Given that there exists a GaAs caplayer, electrons need to first traverse the GaAs X band to couple into the AlGaAs X band. Collector current will not be perceptible until electron kinetic energies reach the AlGaAs X band minimum. In contrast, for secondary electrons generated by inelastic scatterings in the base, their momentum distribution is much less forwardly directed than the incoming distribution. Significant portion of secondary electrons have large $k_{\parallel}$, so they can possibly match four out of the eight L band minima in AlGaAs after traverse the GaAs L band. An example of such momentum matching condition is given in the schematic interface BZ of GaAs (100) in Fig. 10.

VI. ERROR ESTIMATE

For semiconductor band edge determination, besides the fundamental resolution limit set by the thermal broadening of the Fermi distribution, there are several possible sources of errors in the present experimental method. Depending on its origin, each of these errors can be assigned into one of the three categories: sample, measurement, and data analysis. Here, we give a brief discussion on various error sources and their impacts on the precision of the measured barrier heights.

The doping level, composition, and layer thickness of the actual grown sample may be slightly different than the designed structure. It has been known that undoped AlGaAs

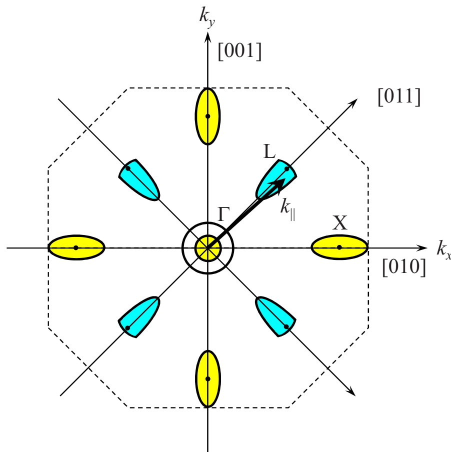

FIG. 10. (Color online) Schematic interface Brillouin zone for GaAs (100). Filled circles and ellipses are the projections of the constant-energy surfaces for electrons near the Γ-, X-, and L-valleys. Dashed octagon outlines the boundary of the projected first Brillouin zone. The arrow exemplifies a possible electron parallel momentum $k_{\|}$ that matches the available states in the L valley.

deposited by MBE contains negative charge.[43] The charge concentration depends on processing and is in the 10^{16} cm^{-3} range. Such unintentional doping in the barrier layer will introduce a band bending and a small overestimate in the measured barrier height. To reduce the sensitivity of barrier heights to unintentional doping, a thinner barrier layer is desired as long as it is not too thin to allow direct tunneling. For GaAs/AlAs HJ, the minimum barrier thickness was found to be 15 nm.[44] A nonuniform unintentional doping across the interested HJ can cause charge transfer and band bending near the HJ, which results in a shift in the observable band offsets. Such a nonuniform doping can be introduced by intrinsic interfacial dipoles that are material and orientation dependent.[45] The compositional error is usually negligible in modern epitaxy techniques. Error in the layer thickness is usually small, except that the surface treatment prior to the Schottky contact deposition and the reaction between the GaAs surface and Al may slightly change the actual GaAs cap-layer thickness. The dopant diffusion from the *p*-doped layer into the undoped layers may slightly reduce the *i* layer thickness, whereas carrier freeze-out at low temperatures may cause a reverse effect. The main impact of errors in the layer thickness is a small change in the slope of the V_C dependence.

Measurement errors are generated from both the external circuitry and the measured device itself, given that care is taken to avoid external noise sources such as mechanical vibration, temperature fluctuation, electromagnetic field, and ground loop. In our setup, the noise floor of the collector current was found to be in the sub-pA level, which is still above the 10 fA resolution limit of the sourcemeter (Keithley 236). Further reduction of the noise floor is possible with measures such as automatic range adjustment. The tunnel transistor device itself may also generate various electronic noises. Thermal or Johnson-Nyquist noise is very small at 4.2 K. Flicker (1/f) noise is the major source of excess low-frequency noise for the present direct current (dc) measurement. In a Schottky diode, both deep-level traps in the depletion region and surface states at the m-s interface can contribute to the low-frequency noise. In the depletion region, the fluctuation in the occupancy of trap states may modulate the barrier height and give rise to a current fluctuation. At low temperatures, tunneling to/from these trap states is the dominant mechanism rather than thermal activation.[46] In several devices, we noticed the appearance of burst noise, also called random telegraph signal (RTS), in the collector current (data not shown). The RTS noise is manifested by steplike switchings between two discrete current levels at random time, with a switching magnitude proportional to the level of collector current. Burst noise has been observed in a large variety of physical systems, whereas its origin is still under debate. In Schottky diodes, it is often attributed to single electron trapping/detrapping at a deep center in the depletion region. Although burst noise itself is an interesting subject to study, it did not occur in most of the measured devices and thus is not concerned in our case.

In the data analysis, numerical errors may be generated by the curve fitting procedure. As we have discussed previously, the slow-rising power-law spectral shape of a BEEM current adds difficulty in determining the turn-on threshold. An empirical power-law fit needs at least three free parameters, and thus introduces a larger standard deviation in the fitted barrier heights than the case of a linear fit that requires only two free parameters. Fitting an experimental spectrum with a fixed power exponent usually generates poorer fitting results. Using a linearization scheme, we have obtained an improved resolution of a few meV in the fitted barrier heights. For materials with unreliable band parameters, such a phenomenological fitting process may give more reliable result than a full-fledged quantum-mechanical calculation.

As a transport method that relies on charge carrier injections, one major source of error is the barrier lowering effects. In most cases one can determine V_{FB} by the polarity reversal of the collected carriers, somehow there are several factors than may introduce uncertainty in such a scheme. Near V_{FB}, it is possible that both electrons and holes are transmitted across the m-s interface. Electron-hole recombinations in the depletion region may nullify the collector current and produce a diverging rise in the apparent turn-on threshold. The image-force lowering with a nonlinear $V_C^{1/2}$ dependence may also become noticeable as the internal E field approaching zero. In our devices, an error of 0.1 V in determining V_{FB} can produce an error of ~5 meV in the measured barrier height. To further reduce the uncertainties due to barrier lowering effects, a larger ratio between the overall thickness of the *i* layer and the depth of the interested HJ is desired to obtain a smaller slope of the E-field dependence.

VII. CONCLUSIONS

As a summary, we have demonstrated a self-consistent way to precisely measure the bandgap of a semiconductor and the band offsets in both the conduction band and the valence band of a semiconductor heterojunction. Using the collector bias as an extra tuning knob, the barrier lowering

effect is naturally taken into account. Excellent agreements with the consensus values are reached by an empirical power-law fitting procedure without requiring *a priori* material parameters. The indirect X and L conduction band minima in AlGaAs are selectively probed by the direct and secondary ballistic electron emission processes, which are explained by the synergetic effect of the drastically different electron momentum distributions generated by these two processes and the parallel momentum conservation at Al/GaAs (100) interface. As a dc technique, a limitation of the present method is the requirement that thermally activated currents over the semiconductor heterojunction need to be suppressed, so that measurements are restricted at low temperatures. Small-signal ac method has been applied to tunnel triodes.[26] In principle, using a narrow-band lock-in amplifier, it is possible to measure a modulated ballistic current in the presence of a large internal current background. Such modulation techniques may allow measurement at higher temperatures as well as probing the band gap of a homogeneous semiconductor without embedded potential steps. Research in this direction is currently being explored.

ACKNOWLEDGMENTS

This work was supported by a DARPA HUNT (Contract No. 222891-01) subaward from the University of Illinois at Urbana-Champaign, the NSF-funded Nanoscale Science and Engineering Center (NSEC), and the Center for Nanoscale Systems (CNS) at Harvard University.

---

*Present address: Information and Quantum Systems Lab, Hewlett-Packard Laboratories, Palo Alto, CA 94304.
weiyi@seas.harvard.edu
†Present address: Department of Electrical and Computer Engineering, University of Utah, Salt Lake City, UT 84112.

[1] For example, see P. Y. Yu and M. Cardona, *Fundamentals of Semiconductors* (Springer, Berlin, 1996).
[2] R. M. Feenstra, Phys. Rev. B **50**, 4561 (1994).
[3] For a review, see E. T. Yu, J. O. McCaldin, and T. C. McGill, in *Solid State Physics*, edited by H. Ehrenreich and D. Turnbull (Academic, New York, 1992), Vol. 46.
[4] R. Dingle, W. Wiegmann, and C. H. Henry, Phys. Rev. Lett. **33**, 827 (1974).
[5] T. M. Ritter, B. A. Weinstein, R. E. Viturro, and D. P. Bour, Phys. Status Solidi B **211**, 869 (1999).
[6] J. Batey and S. L. Wright, J. Appl. Phys. **59**, 200 (1986).
[7] G. W. 'tHooft and S. Colak, Appl. Phys. Lett. **48**, 1525 (1986).
[8] For reviews, see M. Prietsch, Phys. Rep. **253**, 163 (1995); V. Narayanamurti and M. Kozhevnikov, *ibid.* **349**, 447 (2001); J. Smoliner, D. Rakoczy, and M. Kast, Rep. Prog. Phys. **67**, 1863 (2004); W. Yi, A. J. Stollenwerk, and V. Narayanamurti, Surf. Sci. Rep. **64**, 169 (2009).
[9] J. J. O'Shea, E. G. Brazel, M. E. Rubin, S. Bhargava, M. A. Chin, and V. Narayanamurti, Phys. Rev. B **56**, 2026 (1997).
[10] W. Yi, V. Narayanamurti, J. M. O. Zide, S. R. Bank, and A. C. Gossard, Phys. Rev. B **75**, 115333 (2007).
[11] W. Yi, V. Narayanamurti, H. Lu, M. A. Scarpulla, A. C. Gossard, Y. Huang, J.-H. Ryou, and R. D. Dupuis, Appl. Phys. Lett. **95**, 112102 (2009).
[12] N. F. Mott, Math. Proc. Cambridge Philos. Soc. **34**, 568 (1938).
[13] C. A. Mead, Proc. Inst. Radio Engrs. **48**, 359 (1960).
[14] I. Appelbaum, K. J. Russell, V. Narayanamurti, D. J. Monsma, C. M. Marcus, M. P. Hanson, A. C. Gossard, H. Temkin, and C. H. Perry, Appl. Phys. Lett. **82**, 4498 (2003).
[15] A. A. Talin, D. A. A. Ohlberg, R. S. Williams, P. Sullivan, I. Koutselas, B. Williams, and K. L. Kavanagh, Appl. Phys. Lett. **62**, 2965 (1993).
[16] J. C. Fisher and I. Giaever, J. Appl. Phys. **32**, 172 (1961).
[17] J. G. Simmons, J. Appl. Phys. **34**, 1793 (1963).
[18] K. H. Gundlach and J. G. Simmons, Thin Solid Films **4**, 61 (1969).
[19] Z. Hurych, Solid-State Electron. **13**, 683 (1970).
[20] V. Da Costa, F. Bardou, C. Béal, Y. Henry, J. P. Bucher, and K. Ounadjela, J. Appl. Phys. **83**, 6703 (1998).
[21] E. Cimpoiasu, S. K. Tolpygo, X. Liu, N. Simonian, J. E. Lukens, K. K. Likharev, R. F. Klie, and Y. Zhu, J. Appl. Phys. **96**, 1088 (2004).
[22] L. S. Dorneles, D. M. Schaefer, M. Carara, and L. F. Schelp, Appl. Phys. Lett. **82**, 2832 (2003).
[23] M. D. Groner, J. W. Elam, F. H. Fabreguette, and S. M. George, Thin Solid Films **413**, 186 (2002).
[24] A. Davies and H. G. Craighead, Appl. Phys. Lett. **64**, 2833 (1994).
[25] L. B. Leder, M. E. Lasser, and D. C. Rudolph, Appl. Phys. Lett. **5**, 215 (1964).
[26] E. E. Huber, F. L. Johnston, and C. T. Kirk, J. Appl. Phys. **39**, 5104 (1968).
[27] M. H. Hecht, L. D. Bell, W. J. Kaiser, and L. C. Davis, Phys. Rev. B **42**, 7663 (1990).
[28] See revelent chapters in *Properties of Aluminum Gallium Arsenide*, edited by S. Adachi, EMIS Datareviews Series No. 7 (Inspec, London, 1993).
[29] L. D. Bell and W. J. Kaiser, in *Scanning Tunneling Microscopy*, edited by J. A. Stroscio and W. J. Kaiser, Methods of Experimental Physics Vol. 27 (Academic, New York, 1993).
[30] L. D. Bell, M. H. Hecht, W. J. Kaiser, and L. C. Davis, Phys. Rev. Lett. **64**, 2679 (1990).
[31] S. M. Sze, C. R. Crowell, and D. Kahng, J. Appl. Phys. **35**, 2534 (1964).
[32] E. H. Rhoderick, *Metal-Semiconductor Contacts* (Clarendon, Oxford, 1978).
[33] W. Yi, H. Lu, A. C. Gossard, and V. Narayanamurti (unpublished).
[34] V. I. Shashkin and A. V. Murel', Phys. Solid State **50**, 538 (2008).
[35] I. Vurgaftman, J. R. Meyer, and L. R. Ram-Mohan, J. Appl. Phys. **89**, 5815 (2001).
[36] Since the band gap value of GaAs is needed to derive ΔE_C, it is preferable to directly measure it to avoid an uncertainty in the present method. However, such an uncertainty seems to be neg-

ligible since the derived band offset ratio matches extremely well with the 60:40 rule.

[37] S. Oelgart, R. Schwabe, M. Heider, and B. Jacobs, Semicond. Sci. Technol. **2**, 468 (1987).

[38] T. F. Kuech, D. J. Wolford, R. Potemski, J. A. Bradley, K. H. Kelleher, D. Yan, J. Paul Farrell, P. M. S. Lesser, and F. H. Pollak, Appl. Phys. Lett. **51**, 505 (1987).

[39] D. L. Smith, E. Y. Lee, and V. Narayanamurti, Phys. Rev. Lett. **80**, 2433 (1998).

[40] M. Kozhevnikov, V. Narayanamurti, C. Zheng, Yi-Jen Chiu, and D. L. Smith, Phys. Rev. Lett. **82**, 3677 (1999).

[41] K. Maezawa, T. Mizutani, and F. Yanagawa, Jpn. J. Appl. Phys. **25**, L557 (1986).

[42] A. Y. Cho and P. D. Dernier, J. Appl. Phys. **49**, 3328 (1978).

[43] T. W. Hickmott, P. M. Solomon, R. Fischer, and H. Morkoç, J. Appl. Phys. **57**, 2844 (1985).

[44] C. S. Kyono, V. P. Kesan, D. P. Neikirk, C. M. Maziar, and B. G. Streetman, Appl. Phys. Lett. **54**, 549 (1989).

[45] A. Franciosi and C. G. Van de Walle, Surf. Sci. Rep. **25**, 1 (1996).

[46] S. T. Hsu, IEEE Trans. Electron Devices **18**, 882 (1971).